Ultra-low threshold avalanche gain from solar-blind photodetector based on graded-band-gap-cubic-MgZnO

Xiuhua Xie,[1] Zhenzhong Zhang,[1,2] Binghui Li,[1] Shuangpeng Wang,[1] and Dezhen Shen[1,3]

[1]*State Key Laboratory of Luminescence and Applications, Changchun Institute of Optics, Fine Mechanics and Physics, Chinese Academy of Sciences, Changchun 130033, China*

[2]*exciton@163.com*

[3]*shendz@ciomp.ac.cn*

Abstract: A larger ratio of conduction-band offset to valence-band offset is the unique character for $Mg_xZn_{1-x}O$ alloys. For this reason, it is feasible to build a quasi-electric forces, caused by the spatial gradient of the conduction edge, exerting on the electrons. In this paper, a novel graded band gap cubic-MgZnO-based solar-blind photodetector is successfully fabricated from Graded-Band-Gap-Cubic-MgZnO/i-MgO/p-Si heterojunction, via changing stoichiometry spatial gradient. Due to quasi-electric fields in non-uniform MgZnO, the multiple carriers are generated under ultra-low threshold bias voltage. The photodetector showed high performance, namely, high responsivity, quantum efficiency, high sensitivity and selectivity towards the solar-blind spectrum, and fast response times.

OCIS codes: (160.6000) Semiconductor materials; (230.0250) Optoelectronics.

References and links

1. U. Özgur, Y. I. Alivov, C. Liu, A. Teke, M. A. Reshchikov, S. Dogan, V. Avrutin, S. J. Cho, and H. Morkoc, "A comprehensive review of ZnO materials and devices," J. Appl. Phys. **98**(4), 041301 (2005).
2. M. W. Williams and E. T. Arakawa, "Optical properties of single-crystal magnesium oxide," J. Appl. Phys. **38**(13), 5272 (1967).
3. X. L. Du, Z. X. Mei, Z. L. Liu, Y. Guo, T. C. Zhang, Y. N. Hou, Z. Zhang, Q. K. Xue, and A. Y. Kuznetsov, "Controlled growth of high-quality ZnO-based films and fabrication of visible-blind and solar-blind ultra-violet detectors," Adv. Mater. **21**(45), 4625–4630 (2009).
4. W. I. Park, G. C. Yi, M. Kim, and S. J. Pennycook, "Quantum confinement observed in ZnO/ZnMgO nanorod heterostructures," Adv. Mater. **15**(6), 526–529 (2003).
5. R. Chen, B. Ling, X. W. Sun, and H. D. Sun, "Room temperature excitonic whispering gallery mode lasing from high-quality hexagonal ZnO microdisks," Adv. Mater. **23**(19), 2199–2204 (2011).
6. H. Zhu, C. X. Shan, B. Yao, B. H. Li, J. Y. Zhang, Z. Z. Zhang, D. X. Zhao, D. Z. Shen, X. W. Fan, Y. M. Lu, and Z. K. Tang, "Ultralow-threshold laser realized in zinc oxide," Adv. Mater. **21**(16), 1613–1617 (2009).
7. H. Zhu, C. X. Shan, J. Y. Zhang, Z. Z. Zhang, B. H. Li, D. X. Zhao, B. Yao, D. Z. Shen, X. W. Fan, Z. K. Tang, X. Hou, and K. L. Choy, "Low-threshold electrically pumped random lasers," Adv. Mater. **22**(16), 1877–1881 (2010).
8. J. S. Liu, C. X. Shan, B. H. Li, Z. Z. Zhang, K. W. Liu, and D. Z. Shen, "MgZnO p-n heterostructure light-emitting devices," Opt. Lett. **38**(12), 2113–2115 (2013).
9. Z. F. Shi, Y. T. Zhang, X. C. Xia, W. Zhao, H. Wang, L. Zhao, X. Dong, B. L. Zhang, and G. T. Du, "Electrically driven ultraviolet random lasing from an n-MgZnO/i-ZnO/SiO_2/p-Si asymmetric double heterojunction," Nanoscale **5**(11), 5080–5085 (2013).
10. Z. G. Ju, C. X. Shan, D. Y. Jiang, J. Y. Zhang, B. Yao, D. X. Zhao, D. Z. Shen, and X. W. Fan, "$Mg_xZn_{1-x}O$-based photodetectors covering the whole solar-blind spectrum range," Appl. Phys. Lett. **93**(17), 173505 (2008).
11. L. K. Wang, Z. G. Ju, J. Y. Zhang, J. Zheng, D. Z. Shen, B. Yao, D. X. Zhao, Z. Z. Zhang, B. H. Li, and C. X. Shan, "Single-crystalline cubic MgZnO films and their application in deep-ultraviolet optoelectronic devices," Appl. Phys. Lett. **95**(13), 131113 (2009).
12. X. Xie, Z. Zhang, B. Li, S. Wang, M. Jiang, C. Shan, D. Zhao, H. Chen, and D. Shen, "Enhanced solar-blind responsivity of photodetectors based on cubic MgZnO films via gallium doping," Opt. Express **22**(1), 246–253 (2014).
13. Y. N. Hou, Z. X. Mei, Z. L. Liu, T. C. Zhang, and X. L. Du, "$Mg_{0.55}Zn_{0.45}O$ solar-blind ultraviolet detector with high photoresponse performance and large internal gain," Appl. Phys. Lett. **98**(10), 103506 (2011).

#250209 Received 16 Sep 2015; revised 23 Nov 2015; accepted 27 Nov 2015; published 8 Dec 2015

14. H. L. Liang, Z. X. Mei, Q. H. Zhang, L. Gu, S. Liang, Y. N. Hou, D. Q. Ye, C. Z. Gu, R. C. Yu, and X. L. Du, "Interface engineering of high-Mg-content MgZnO/BeO/Si for p-n heterojunction solar-blind ultraviolet photodetectors," Appl. Phys. Lett. **98**(22), 221902 (2011).
15. G. Konstantatos and E. H. Sargent, "Nanostructured materials for photon detection," Nat. Nanotechnol. **5**(6), 391–400 (2010).
16. H. Kroemer, "Quasi-electric and quasi-magnetic fields in nonuniform semiconductors," RCA Rev. **18**, 332 (1957).
17. B. Laumer, F. Schuster, T. A. Wassner, M. Stutzmann, M. Rohnke, J. Schormann, and M. Eickhoff, "ZnO/(ZnMg)O single quantum wells with high Mg content graded barriers," J. Appl. Phys. **111**(11), 113504 (2012).
18. X. Zhuang, C. Z. Ning, and A. Pan, "Composition and bandgap-graded semiconductor alloy nanowires," Adv. Mater. **24**(1), 13–33 (2012).
19. L. Li, H. Lu, Z. Yang, L. Tong, Y. Bando, and D. Golberg, "Bandgap-graded CdS_xSe_{1-x} nanowires for high-performance field-effect transistors and solar cells," Adv. Mater. **25**(8), 1109–1113 (2013).
20. Y. Lu, F. Gu, C. Meng, H. Yu, Y. Ma, W. Fang, and L. Tong, "Multicolour laser from a single bandgap-graded CdSSe alloy nanoribbon," Opt. Express **21**(19), 22314–22319 (2013).
21. Y. Y. Lai, Y. P. Lan, and T. C. Lu, "Strong light-matter interaction in ZnO microcavities," Light Sci. Appl. **2**(6), e76 (2013).
22. A. Ohtomo, M. Kawasaki, I. Ohkubo, H. Koinuma, T. Yasuda, and Y. Segawa, "Structure and optical properties of $ZnO/Mg_{0.2}Zn_{0.8}O$ superlattices," Appl. Phys. Lett. **75**(7), 980 (1999).
23. Y. F. Li, B. Yao, Y. M. Lu, B. H. Li, Y. Q. Gai, C. X. Cong, Z. Z. Zhang, D. X. Zhao, J. Y. Zhang, D. Z. Shen, and X. W. Fan, "Valence-band offset of epitaxial ZnO/MgO (111) heterojunction determined by x-ray photoelectron spectroscopy," Appl. Phys. Lett. **92**(19), 192116 (2008).
24. C. G. Van de Walle and J. Neugebauer, "Universal alignment of hydrogen levels in semiconductors, insulators and solutions," Nature **423**(6940), 626–628 (2003).
25. Y. Z. Zhu, G. D. Chen, H. G. Ye, A. Walsh, C. Y. Moon, and S. H. Wei, "Electronic structure and phase stability of MgO, ZnO, CdO, and related ternary alloys," Phys. Rev. B **77**(24), 245209 (2008).
26. P. D. C. King, T. D. Veal, A. Schleife, J. Zuniga-Perez, B. Martel, P. H. Jefferson, F. Fuchs, V. Munoz-Sanjose, F. Bechstedt, and C. F. McConville, "Valence-band electronic structure of CdO, ZnO, and MgO from x-ray photoemission spectroscopy and quasi-particle-corrected density-functional theory calculations," Phys. Rev. B **79**(20), 205205 (2009).
27. R. Dahal, T. M. Al Tahtamouni, J. Y. Lin, and H. X. Jiang, "AlN avalanche photodetectors," Appl. Phys. Lett. **91**(24), 243503 (2007).
28. X. H. Xie, Z. Z. Zhang, C. X. Shan, H. Y. Chen, and D. Z. Shen, "Dual-color ultraviolet photodetector based on mixed-phase-MgZnO/i-MgO/p-Si double heterojunction," Appl. Phys. Lett. **101**(8), 081104 (2012).
29. D. G. Baik and S. M. Cho, "Application of sol-gel derived films for ZnO/n-Si junction solar cells," Thin Solid Films **354**(1), 227–231 (1999).
30. J. Yamashita, "Oxygen band in magnesium oxide," Phys. Rev. **111**(3), 733–735 (1958).
31. J. Liang, H. Z. Wu, Y. F. Lao, N. B. Chen, P. Yu, and T. N. Xu, "Characterization of cubic phase MgZnO/Si(100) interfaces," Appl. Surf. Sci. **252**(4), 1147–1152 (2005).
32. T. C. Zhang, Y. Guo, Z. X. Mei, C. Z. Gu, and X. L. Du, "Visible-blind ultraviolet photodetector based on double heterojunction of n-ZnO/insulator-MgO/p-Si," Appl. Phys. Lett. **94**(11), 113508 (2009).

1. Introduction

As a member of group $II^{(a,b)}$-VI wide-band-gap semiconductors, $Mg_xZn_{1-x}O$ alloys are generating considerable interest as they can provide, in principle, an accessible band-gap range from around 3.37 eV (ZnO) to 7.8 eV (MgO) [1,2]. This makes them promising candidates for deep ultraviolet (DUV) optoelectronic devices [3–6]. Random lasers, light-emitting diodes based on MgZnO alloys have been successfully demonstrated [7–9]. In the past decade, a large number of experiments have been conducted, focusing on solar-blind photodetection using MgZnO films, because of various important applications in missile tracking, flame detection, ozone layer monitoring, and so on [10–14]. To date, however, most of the solar-blind photodetectors based on MgZnO have low-performance, especially in responsivity, which is one of the important figures of merit for DUV detectors to be commercially applied [15]. Consequently, a controllable and high gain mechanism is required.

Graded-band-gap is an energy band gap that varies with position, produced by spatially varying the stoichiometry of a semiconductor, which was first proposed by Kroemer [16]. The quasi-electric forces, caused by the spatial gradient of the conduction and valence band edge, are exerted on the electrons and holes, respectively. Then, some excellent optical detectors and other devices based on graded-band-gap semiconductors had been obtained [17–21]. For $Mg_xZn_{1-x}O$ alloys, due to the wide tunable bandgap and a larger ratio of conduction-band

#250209 Received 16 Sep 2015; revised 23 Nov 2015; accepted 27 Nov 2015; published 8 Dec 2015

offset to valence-band offset ($\Delta E_C/\Delta E_V$) [22,23], it is very suitable for photon detection by using graded-band-gap technique. Further, the cubic-MgZnO is of octahedral coordination in the cubic rocksalt (RS) structure. Due to the larger bond length of Mg-O compared to Zn-O in this ionic system, the valence band maximum (VBM) of RS-ZnO is slightly lower than RS-MgO [24–26], which makes quasi-electric forces for electrons in graded-band-gap become much more marked than for holes. However, graded-band-gap-cubic-MgZnO (GBGC-MgZnO) based devices (in particular, DUV photodetectors) have rarely been studied.

Motivated by the above reasons, in this work, via constructing heterojunctions based on GBGC-MgZnO/i-MgO/p-Si, we demonstrated a solar-blind photodetector with enhanced and tunable gain under ultra-low threshold bias voltage. The photodetector showed sensitive spectral response, high quantum efficiency, and fast response time. The gain mechanism of the device was discussed in detail.

2. Experiment

The GBGC-MgZnO film was grown on a p-type Si (111) (resistivity 18 ohm•cm and carrier concentration ~10^{18}cm^{-3}) substrate with a MgO buffer layer about 30 nm by metal-organic chemical vapor deposition (MOCVD). Polished p-type silicon substrates were cleaned by RCA method. Oxygen (O_2), Diethylzinc (DEZn), and Dimethyl dicyclopentadienyl magnesium ($MeCp_2Mg$) were employed as the precursors. Nitrogen with 6N-purity was used as the carrier gas. The GBGC-MgZnO was grown at 450 °C with keeping the chamber pressure at 150 Torr. A reference GBGC-MgZnO film grown on a c-plane sapphire substrate with the same growth conditions was used to examine optical bandgap and Ohmic contact of metal electrodes on the film. The flux ratio for [$MeCp_2Mg$] and [DEZn] was monotonically decreasing, during the growth process. The structure characterization of the film was evaluated by an x-ray diffraction (XRD) with Cu-K_α 0.154 nm line as the radiation source. The morphology of the GBGC-MgZnO film (top view) was examined with a scanning electron microscope (SEM) (HITACHI S-4800).

A circular Indium film (~400 nm) and a gold film (~80 nm) were deposited on the backside of the p-Si substrate and GBGC-MgZnO as the electrodes, respectively, by thermal evaporation method. Hall measurement system (Lakeshore HMS7707) was utilized for current-voltage (I-V) characterization of the photodetector. The spectral response of the solar-blind photodetector was measured using a 150 W Xe lamp, a monochromator, an optical chopper (EG&G 192), and a lock-in amplifier (EG&G 124A) in a synchronous detection scheme. A UV-enhanced Si detector was employed to calibrate the system. The time resolved response of the photodetector was obtained using an oscilloscope (500 MHz) and a YAG:Nd laser with a wavelength of 266 nm (50 mJ) and a pulse width of 10 ns.

3. Results and discussion

The X-ray diffraction (XRD) pattern in Fig. 1(a) shows only one peak corresponding to (111) diffraction of cubic MgZnO besides the diffraction from silicon substrate. It reveals that the graded-band-gap film is single cubic structure without other phase (e.x. wurtzite). As seen from the scanning electron microscope (SEM) image in Fig. 1(b), the GBGC-MgZnO film shows clear cubic feature with (111) orientation, which is in accordance with the XRD pattern. The epitaxial film is about 280 nm thick, as measured by the cross section view SEM image in Fig. 1(c). It provides a basis for realizing a larger quasi-electric forces acting on the electrons. A line-scan profile of energy dispersive X-ray spectra (EDX), which is along the growth direction of the film, is illustrated in Fig. 1(d). As seen, the Mg fraction ([Mg]) decreases along the growth direction, while the [Zn] increases and [O] keeps constant. It indicates that the graded-band-gap film has indeed been achieved.

#250209 Received 16 Sep 2015; revised 23 Nov 2015; accepted 27 Nov 2015; published 8 Dec 2015

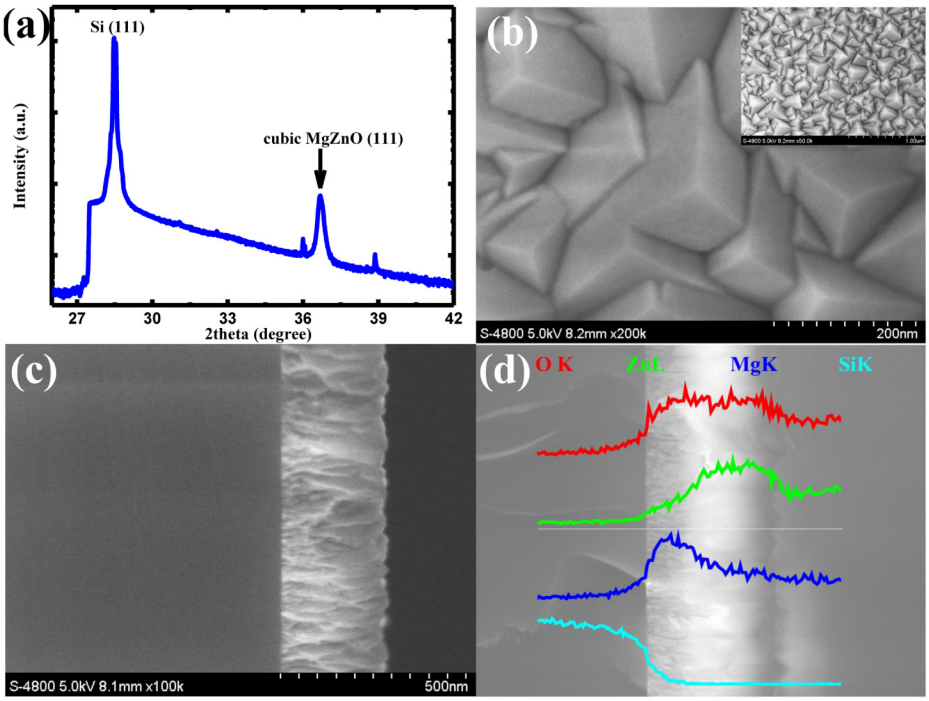

Fig. 1. (a) XRD pattern of the heterostructure. SEM image of the GBGC-MgZnO film (b) top view and (c) side view. (d) Line-scan profile across the growth direction of the film.

By evaporating the electrodes on both the sides, DUV photodetectors were achieved, as sketched in Fig. 2(a). The heterojunctions show significant rectification characteristics under dark conditions, with an open voltage of about 2 V, as shown in Fig. 2(b). Before breakdown at ~10V, the reverse current-voltage characteristics and the saturation current (I0) show a slowly increasing trend. It suggests that there is multiplication mechanism present (see below for further discussion). No doubt the resulting gain is beneficial to photon detection. The inset of Fig. 2(c) shows the dark current (I_{dark}) and photocurrent (I_{photo}) dependences on the reverse bias. A large ratio of I_{photo}/ I_{dark} can be observed. In general, the multiplication gain is calculated from the unity gain response by the express $G(V) = [I_{photo}(V) - I_{dark}(V)]/ [I_{photo}(V_G = 1) - I_{dark}(V_G = 1)]$, where G is the gain at a certain reverse bias V [27]. The device, as shown in Fig. 2(c), exhibits a nonlinear increasing gain versus bias. The maximum gain exceeds 10, which is larger than that observed for homogeneous MgZnO solar-blind photodetector [11,28].

The photoresponse spectra of the GBGC-MgZnO devices were measured. Figure 3(a) illustrates the spectral response measured at a 1.0-V bias at room-temperature. The photodetectors show a high sensitivity to solar-blind light with a typical cutoff wavelength of about 280 nm, which corresponds to the optical transmission spectrum measured on the reference GBGC-MgZnO film grown on a c-plane sapphire substrate. It is shown that the (Reponsivity @ 240nm)/(Responsivity @ 600nm) is about two orders of magnitude, demonstrating the good DUV performance of the photodetector. The photoresponse spectra at various reverse biases are shown in Fig. 3(b). The responsivity increases significantly with increasing the reverse bias. As seen in the inset of Fig. 3(b), the peak responsivity, at 240 nm, shows a nonlinear rising with increasing the bias. The quantum efficiency is up to ~600% at a 6 V bias.

#250209 Received 16 Sep 2015; revised 23 Nov 2015; accepted 27 Nov 2015; published 8 Dec 2015

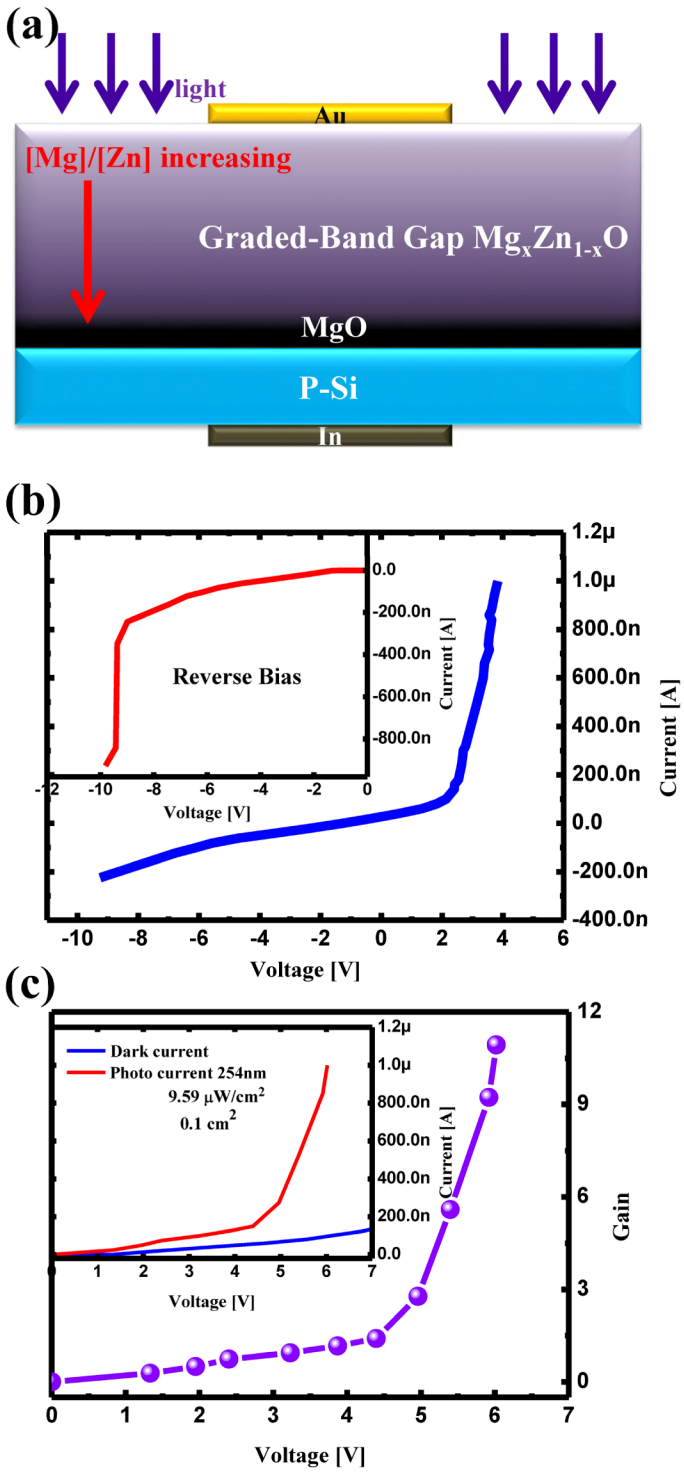

Fig. 2. (a) The schematic of the detector for measuring photoresponse. (b) I-V curve of the detector under dark condition at room temperature. The reverse current-voltage is magnified in the inset. (c) Gain extracted from the photocurrent measurements. The inset is reverse I-V characteristics of the detector in dark and under 254 nm light illumination.

#250209 Received 16 Sep 2015; revised 23 Nov 2015; accepted 27 Nov 2015; published 8 Dec 2015

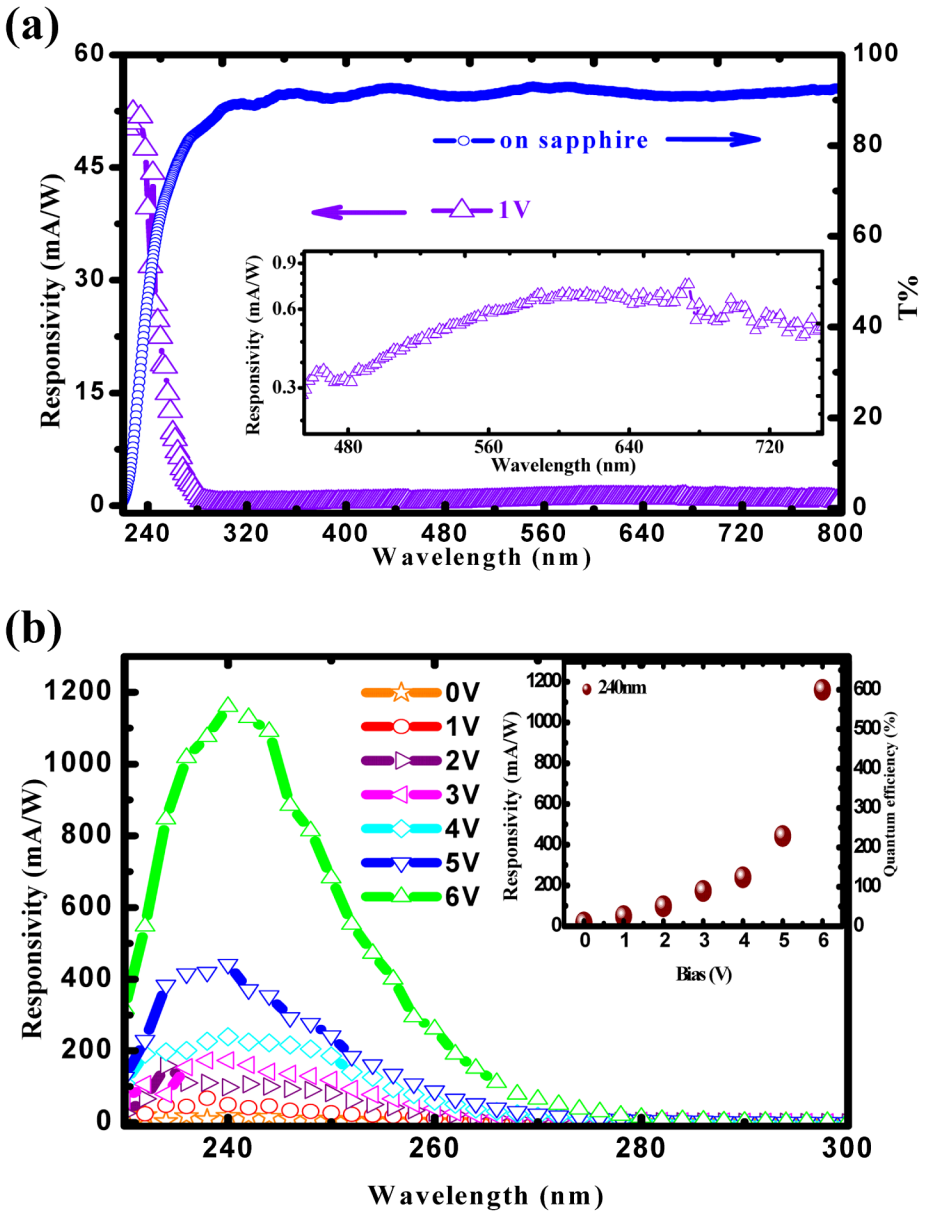

Fig. 3. (a) Transmission data (blue circle) from reference GBGC-MgZnO film grown on a c-plane sapphire. The spectral response (violet triangle) of the detector under 1 V. (b) Responsivity of the photodetector for different reverse bias voltages.

Figure 4(a) shows a series of impulse responses of the photodetector with a load resistance of 50 ohm. The device shows a fast photoresponse. The decay time of the detector versus reverse bias is plotted in Fig. 4(b). As the bias is beyond 4 V, the decay time stays almost constant, due to carriers reaching their saturation velocity as well as to the intrinsic time delays associated with multiplication process.

#250209 Received 16 Sep 2015; revised 23 Nov 2015; accepted 27 Nov 2015; published 8 Dec 2015

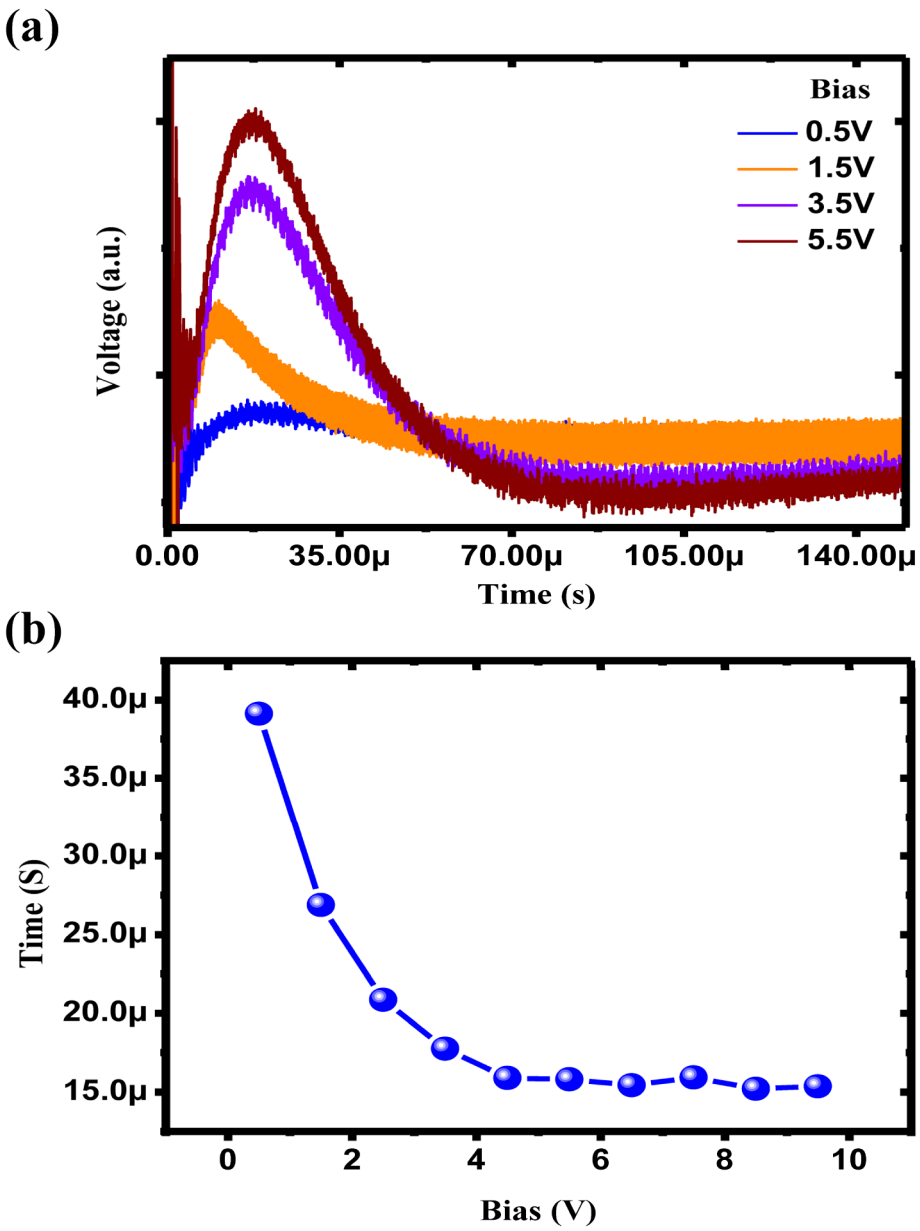

Fig. 4. Time-resolved photocurrent measurements. (a) Photocurrent transients measured on the photodetector at different biases. (b) Decay time for different bias voltages.

Figure 5 shows the band diagrams derived from the Anderson model to further analyze the gain mechanisms of the GBGC-MgZnO based photodetector. According to the band gap of 1.12, 7.8 eV and electron affinity (χ) of 4.05, 0.8 eV for Si and MgO, respectively, the conduction band offset at the Si/MgO interface is calculated to be 3.2 eV [29–31]. Under thermal equilibrium [Fig. 5(a)], as a result of carrier diffusion, the depletion regions will be formed in both Si and GBGC-MgZnO sides. The Fermi level becomes constant across the entire region of the heterostructure. By varying [Mg] and [Zn], a considerable spatial gradient of the conduction band edge was formed in GBGC-MgZnO side due to the larger ratio of $\Delta E_C/\Delta E_V$. It can supply a quasi-electric force exerting on the electrons. As depicted in the schematic in Fig. 5(b), when the photodetector is under illumination, the photogenerated

#250209 Received 16 Sep 2015; revised 23 Nov 2015; accepted 27 Nov 2015; published 8 Dec 2015

carriers will be driven by the built-in electric field. However, due to the high barrier (3.2 eV), the visible-light generated electrons from p-Si side cannot cross over the (p-Si)/(i-MgO) interface, and then recombine with holes immediately. Therefore, the visible-light response from Si substrate was suppressed [32]. On the other side, thanks to the large quasi-electric forces, photogenerated electron-hole in the GBGC-MgZnO layer will be efficiently separated. And then the holes transmit through the i-MgO layer because of the relatively low barrier. Meanwhile, the electrons are multiplied through impact ionization with the reverse bias increasing, because of the larger electric field. Indeed, as opposed to the conventional p–i–n diodes, the use of graded-band-gap produces high electric fields by using an extremely large content spatial gradient. The electric field strength in the GBGC-MgZnO layer is proximity ~10^6 V/cm, suggesting a high probability of impact ionization.

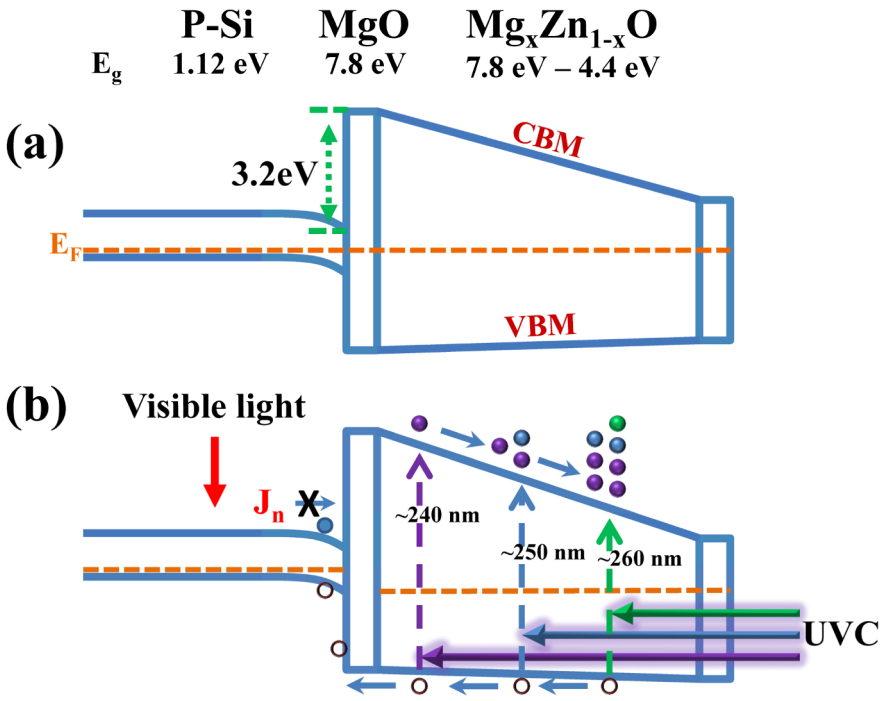

Fig. 5. Schematic diagram showing the band alignment of the heterojunction (a) under equilibrium condition (b) under illumination at reverse bias.

4. Conclusion

In summary, we have demonstrated an effective approach to improve responsivity with enhanced and tunable gain, under ultra-low threshold bias voltage, via changing stoichiometry spatial gradient. The photodetector showed high performance under low reverse bias voltage (6 V), namely, high responsivity (1160 mA/W@240nm), quantum efficiency (600%@240 nm), high sensitivity and selectivity towards the solar-blind spectrum, and fast response times (~15 μs@266nm). The Graded-Band-Gap-Cubic-MgZnO, in addition, will be more valuable in the field of low-noise solar-blind detection for its significant band alignment different between the conduction band and valence band.

Acknowledgments

This work is supported by the National Basic Research Program of China (973 Program) under No.s 2011CB302006 and 2011CB302002, the National Natural Science Foundation of China under No.s 11134009, 61376054, 61425021 and 61525404, the 100 Talents Program of the Chinese Academy of Sciences.

#250209 Received 16 Sep 2015; revised 23 Nov 2015; accepted 27 Nov 2015; published 8 Dec 2015